

Summary of the ASK14 Ground Motion Relation for Active Crustal Regions

Norman A. Abrahamson,^{a)} M.EERI, Walter J. Silva,^{b)} M.EERI,
and Ronnie Kamai,^{c)} M.EERI

Empirical ground motion models for the average horizontal component from shallow crustal earthquakes in active tectonic regions are derived using the PEER NGA-West2 database. The model is applicable to magnitudes 3.0–8.5, distances 0–300 km, and spectral periods of 0–10 s. The model input parameters are the same as those used by Abrahamson and Silva (2008), with the following exceptions: the loading level for nonlinear effects is based on the spectral acceleration at the period of interest rather than the PGA; and the distance scaling for hanging wall (HW) effects off the ends of the rupture includes a dependence on the source-to-site azimuth. Regional differences in large-distance attenuation and V_{S30} scaling between California, Japan, China, and Taiwan are included. The scaling for the HW effect is improved using constraints from numerical simulations. The standard deviation is magnitude-dependent, with smaller magnitudes leading to larger standard deviations at short periods, but smaller standard deviations at long periods. Directivity effects are not included through explicit parameters, but are captured through the variability of the empirical data. [DOI: 10.1193/070913EQS198M]

INTRODUCTION

We present an update (denoted as ASK14) to the [Abrahamson and Silva \(2008\)](#); denoted as AS08) ground motion prediction equation (GMPE), based on the NGA-West2 database ([Ancheta et al. 2014](#)). The model is cast in terms of the new rotated measure that is used in all NGA-West2 models: RotD050, the 50th percentile of the response spectra over all non-redundant rotation angles. Further explanation on the new intensity measure is provided in [Boore \(2010\)](#). In this paper, we summarize the ASK14 model. Complete descriptions of the basis for the selection of the data set, the basis for the functional form of the ground motion model, the details of the regression analysis, and a comprehensive set of residual plots are given in [Abrahamson et al. \(2013\)](#).

A full set of the final model coefficients is listed in Tables 4 through 7 and is also attached as an Electronic Supplement in the online version of this paper. Note that the coefficients published in the PEER report ([Abrahamson et al. 2013](#)) have been updated, and further smoothing was applied to address three main issues that were found during the time period following the publication of the report. The additional smoothing addresses the following:

^{a)} Pacific Gas & Electric Company, 245 Market Street, San Francisco, CA 94105

^{b)} Pacific Engineering and Analysis, 311 Pomona Ave, El Cerrito, CA 94546

^{c)} Ben-Gurion University of the Negev, Israel, 84105

(1) The spectral shape remains smooth at short distances, (2) the spectral displacement flattens out at long periods for small magnitudes, and (3) the high-frequency shape does not dip below the PGA out to 300 km.

The development of GMPEs for use in hazard studies is not simple curve fitting, but rather, it is model building, which uses results from seismological and geotechnical numerical modeling, in addition to the empirical ground motion data, to develop the models. In developing our GMPE, apart from the empirical NGA-West2 database ([Ancheta et al. 2014](#)), we have made use of the results from one-dimensional (1-D) finite-fault kinematic simulations to constrain the hanging wall (HW) scaling ([Donahue and Abrahamson 2014](#)), 1-D finite-fault kinematic source models for M 6.5 to M 8.25 to constrain the large-magnitude scaling ([Collins et al. 2006](#)), and equivalent-linear analytical models of site response to constrain the nonlinear site response scaling ([Kamai et al. 2014](#)).

A common comment about the AS08 model is that it is too complicated and that there is not adequate empirical data to constrain all of the parameters in the model. As will be shown, the complex functional form is needed so that the GMPE extrapolates in a realistic manner for short distances and large magnitudes, which are not well constrained in the empirical data. In particular, the complexity of the functional form is primarily due to the HW effects and the nonlinear site response effects (on both the median and the standard deviation), which are both constrained by numerical simulation results.

The full functional form, which will be described below, is coded into Matlab and is provided as an electronic supplement to this paper, titled “ASK14.m.” The required list of coefficients in the format read by the code is also provided in the file “ASK14_coeffs.m.”

DATA SET SELECTION

We selected our ground motion data set from the NGA-West2 database ([Ancheta et al. 2014](#)). Our general approach for selecting the subset of data for use in the regression analysis was to include all earthquakes, including Class 2 earthquakes (for a definition of Class 2, see the section “Aftershock Scaling” section below, as well as [Wooddell and Abrahamson 2014](#)), in active crustal regions (ACRs) under the assumption that the median ground motions in ACRs at distances less than about 80 km are similar around the world. In the context of simple source models, we are assuming that median stress-drops are similar for earthquakes in different ACRs (e.g., California, Alaska, Taiwan, Japan, Turkey, Italy, Greece, New Zealand, Northwest China). We tested the validity of this assumption by comparing the inter-event residuals from earthquakes in other regions with those from earthquakes in California ([Abrahamson and Silva 2007](#)).

While recordings from poorly sampled regions are limited to a maximum distance of 80 km, recordings from California, China, Taiwan, and Japan are extended to 400 km. At distances greater than 80 km, differences in crustal structure can have significant effects on the ground motions, leading to a change in the attenuation at large distances (e.g., Q term). Regional differences are included in the GMPE to account for such differences.

A summary of the criteria for excluding earthquakes and recordings is given below. The details of the selection are described in [Abrahamson et al. \(2013\)](#):

- Remove earthquakes not representative of ACRs.
- Remove earthquakes with questionable hypocentral depths.
- Remove earthquakes with fewer than three recordings for $M > 5$ and earthquakes with fewer than ten recordings with good coverage in distance for earthquakes with $M < 5$. The difference in magnitude ranges is due to the abundance of small-magnitude data in the database.
- Remove the Wenchuan aftershocks. During our preliminary evaluations, we found that the residuals and spectral shape of the Wenchuan aftershocks were very different from other regions, which may reflect unreliable metadata for these events. While we included the Wenchuan main shock, we removed the aftershocks.
- Remove recordings not representative of free-field ground motion.
- Remove recordings missing key metadata.
- Remove recordings identified as questionable (i.e., apparent incorrect gain or spectral shape, as flagged in the NGA-West2 flatfile; see [Ancheta et al. 2014](#) for examples).
- Remove recordings at distances greater than censoring distance. The censoring distance is year- and magnitude-dependent and was developed to address the incompleteness of the data set, typically due to triggering threshold in old instrumentation. A full explanation is given in [Abrahamson et al. \(2013\)](#).

Our final data set consists of 15,750 recordings from 326 earthquakes, 221 of which are strike-slip events, 79 of which are reverse events (both covering the entire magnitude range), and 26 of which are normal events, mostly within $4.6 < M < 6$. The distribution of recordings by region is given in Table 1. The magnitude and distance distribution is shown in Figure 1.

The response spectral values for the selected recordings are only used in the regression analysis for spectral frequencies greater than 1.25 times the high-pass corner frequency used

Table 1. Summary of selected subset by region

Region no.	Region	No. of earthquakes	Magnitude range	Distance range (km)	Total no. of recordings
1	California	274	3.1–7.3	0.07–345	12,044
2	Other WUS	2	5.1–7.9	2.7–54.8	7
3	Taiwan	6	5.9–7.6	0.6–172.2	1,535
4	Italy	25	4.0–6.9	3.8–75.7	175
5	Middle East	5	6.6–7.5	0.2–75.6	43
6	Central America	0	—	—	0
7	New Zealand	2	6.2–7.0	1.2–79.5	72
8	Europe (excluding Italy and Greece)	1	7.1	4.4–66.7	6
9	China	4	4.8–7.9	0.05–348.9	158
10	Japan	5	6.1–6.9	0.3–300.1	1,700
11	Greece	1	6.4	19.5–79.4	3
12	Other	1	6.2	31.5–63.6	5

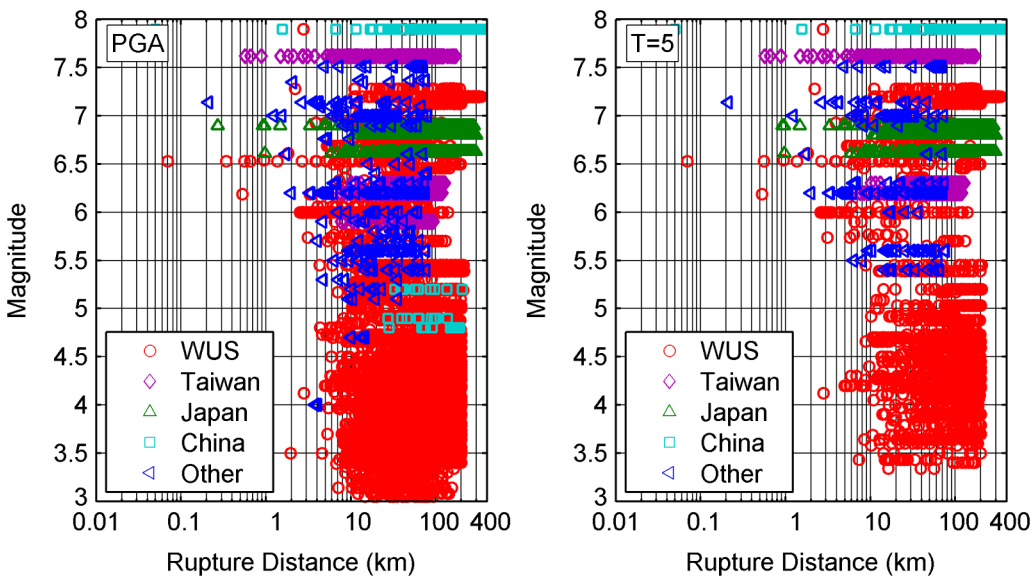


Figure 1. Distribution of magnitude-distance pairs for PGA and $T = 5$ s.

in the record processing, as defined in the NGA-West2 database. This requirement produces a data set that varies as a function of period. The period dependence of the number of earthquakes and number of recordings used in the regression analysis is shown in Figure 2. The steps to which Figure 2 refers are regression steps with increasing magnitude and distance ranges, as follows:

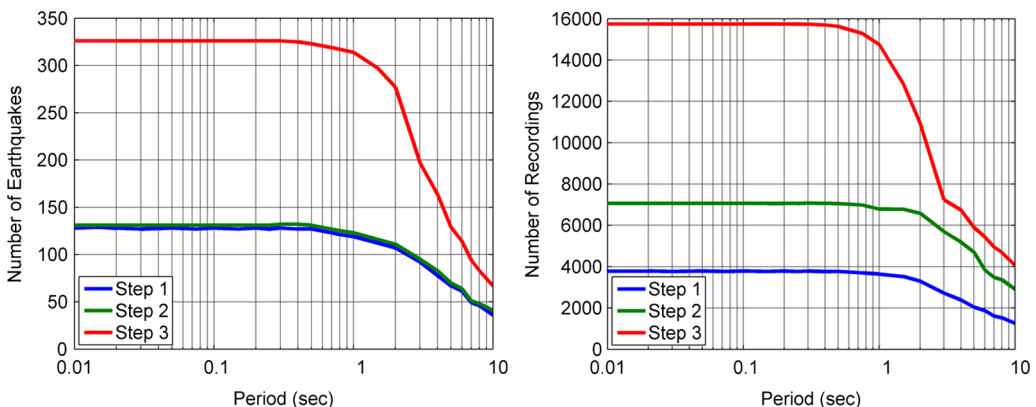


Figure 2. Period dependence of the number of earthquakes and the number of recordings in our subset based on the lowest usable frequency for the average horizontal component listed in the flat-file.

- Step 1: $M > 4.5$, $R_{RUP} < 80$ km.
- Step 2: $M > 4.5$, $R_{RUP} < 300$ for CA, Japan, and Taiwan; $R_{RUP} < 80$ for others.
- Step 3: $M > 3$, $R_{RUP} < 300$ for CA, Japan, and Taiwan; $R_{RUP} < 80$ for others.

SITE CLASSIFICATION

The site condition is classified using two parameters: the average shear-wave velocity in the top 30 m (V_{S30}) and the depth to $V_S = 1.0$ km/s (Z_1). This does not imply that 30 m is the key depth range for the site response, but rather that V_{S30} is correlated with the deeper velocity structure that controls the site amplification. Because the correlation between V_{S30} and the deeper structure may vary from region to region, we allowed the scaling with V_{S30} to be region-dependent. Using the soil depth, in addition to V_{S30} , allows the ground motion model to distinguish between shallow soil sites and deep soil sites with the same V_{S30} . Although the depth to 2.5 km/s ($Z_{2.5}$) may be more directly related to the long-period site response, we selected Z_1 because it is closer to the traditional geotechnical parameter of “depth to bedrock” and is easier to measure for specific projects.

DISTANCE DEFINITION

As with the AS08 model, we use the closest distance to the rupture plane, R_{RUP} , as the primary distance measure. Four additional distance measures, R_{JB} , R_x , R_1 , and R_{y0} , are used to model the attenuation of HW effects: R_{JB} is the closest horizontal distance to the surface projection of the rupture; R_x is the horizontal distance from the top edge of the rupture, measured perpendicular to the fault strike; R_1 is the value of R_x at the bottom edge of the rupture; and R_{y0} is the horizontal distance off the end of the rupture measured parallel to strike (see [Kaklamanos et al. 2011](#) for illustrations of all but R_{y0}). In the NGA-West2 database, events without a finite fault model but with minimal information on hypocenter, magnitude, and fault plane solution (see [Ancheta et al. 2014](#)) use simulated finite fault planes. For small-magnitude events ($< M 4.5$), this results in R_{RUP} and R_{JB} approximately equal to the hypocentral distance.

DEFINITION OF REFERENCE ROCK CONDITIONS AND GROUND MOTION LEVEL

The reference rock conditions are defined at $V_{S30} = 1,180$ m/s, which is an update to the AS08 model that used 1,100 m/s as the reference rock. This updated value is more accurate with respect to the values used in the 1-D site response simulations; however, the effect of changing the reference rock from 1,100 to 1,180 has an insignificant effect on the nonlinear site response in the model. There is no change in the linear scaling either, since the linear scaling is a result of the regression and it will adjust to the reference value used in the regression.

Nonlinear site effects will depend on the level of ground motion. [Kamai et al. \(2014\)](#) developed nonlinear site amplification models for two different measures of the level of shaking: the peak acceleration and the spectral acceleration on rock ($V_{S30} = 1,180$ m/s) at the period of interest. [Kamai et al. \(2014\)](#) showed that both parameters work about equally well. We selected the spectral acceleration on rock because it simplifies the model for the standard deviation as the correlation of peak acceleration and spectral acceleration is no longer needed.

FUNCTIONAL FORM OF THE MODEL

There are four key changes to the functional form, when compared to AS08: (1) The model is extended to small magnitudes ($\mathbf{M} < 3$), requiring another break in the magnitude scaling; (2) the HW scaling is better constrained by simulations; (3) regional differences in the large distance attenuation (linear R term) are included; and (4) regional differences in the V_{S30} scaling are included. We believe that these changes represent major improvements to our previous ground motion model that justify the additional complexity in our model.

EQUATIONS FOR THE MEDIAN GROUND MOTION

The model for the median ground motion is given by:

$$\begin{aligned} \ln Sa(g) = & f_1(\mathbf{M}, R_{RUP}) + F_{RV}f_7(\mathbf{M}) + F_Nf_8(\mathbf{M}) + F_{As}f_{11}(CR_{JB}) \\ & + f_5(\widehat{Sa}_{1180}, V_{S30}) + F_{HW}f_4(R_{JB}, R_{RUP}, R_x, R_{y0}, W, dip, Z_{TOR}, \mathbf{M}) \\ & + f_6(Z_{TOR}) + f_{10}(Z_1, V_{S30}) + \text{Regional}(V_{S30}, R_{RUP}) \end{aligned} \quad (1)$$

The parameters in Equation 1 are defined in Table 2.

The functional forms for f_1 , f_4 , f_5 , f_6 , f_7 , f_8 , f_{10} , f_{11} , and the regional term are given below.

Basic Form

The basic form of the magnitude and distance dependence for strike-slip earthquakes is similar to our 2008 model, with an additional break in the magnitude scaling for small magnitudes ($\mathbf{M} < 5$):

$$f_1 = \begin{cases} a_1 + a_5(\mathbf{M} - M_1) + a_8(8.5 - \mathbf{M})^2 + [a_2 + a_3(\mathbf{M} - M_1)]\ln(R) + a_{17}R_{RUP} & \text{for } \mathbf{M} > M_1 \\ a_1 + a_4(\mathbf{M} - M_1) + a_8(8.5 - \mathbf{M})^2 + [a_2 + a_3(\mathbf{M} - M_1)]\ln(R) + a_{17}R_{RUP} & \text{for } M_2 \leq \mathbf{M} < M_1 \\ a_1 + a_4(M_2 - M_1) + a_8(8.5 - M_2)^2 + a_6(\mathbf{M} - M_2) \\ + a_7(\mathbf{M} - M_2)^2 + [a_2 + a_3(M_2 - M_1)]\ln(R) + a_{17}R_{RUP} & \text{for } \mathbf{M} < M_2 \end{cases} \quad (2)$$

where

$$R = \sqrt{R_{RUP}^2 + c_{4M}^2} \quad (3)$$

The term that is added to R_{RUP} inside the square root is typically referred to as the “fictitious depth,” due to the way it affects the distance term. While the fictitious depth in AS08 was a constant, we modify it in ASK14 to reduce to 1 km at small magnitudes, as follows:

$$c_{4M}(\mathbf{M}) = \begin{cases} c_4 & \text{for } \mathbf{M} > 5 \\ c_4 - (c_4 - 1)(5 - \mathbf{M}) & \text{for } 4 < \mathbf{M} \leq 5 \\ 1 & \text{for } \mathbf{M} \leq 4 \end{cases} \quad (4)$$

Table 2. Definition of parameters used in the regression analysis

Parameter	Definition	Notes
<i>Source definition</i>		
M	Moment magnitude	
CR_{JB}	Centroid R_{JB} (see the “Aftershock Scaling” section here or Wooddell and Abrahamson 2014 for a detailed explanation)	Class 2 events are those with $CR_{JB} < 15$ km, and within the Gardner and Knopoff (1974) time window
Z_{TOR}	Depth to top of rupture (km)	
F_{RV}	Flag for reverse faulting earthquakes	1 for reverse and reverse/oblique earthquakes defined by rake angles between 30 and 150 degrees, 0 otherwise
F_N	Flag for normal faulting earthquakes	1 for normal earthquakes defined by rake angles between -30 and -150 degrees, 0 otherwise
F_{AS}	Flag for aftershocks	1 for Class 2, 0 for Class 1
<i>Distance definition</i>		
R_{RUP}	Rupture distance (km)	
<i>Site model</i>		
V_{S30}	Shear-wave velocity over the top 30 m (m/s)	
Z_1	Depth to $V_S = 1.0$ km/s at the site (m)	
\widehat{Sa}_{1180}	Median peak spectral acceleration (g) for $V_{S30} = 1,180$ m/s	
<i>HW model</i>		
F_{HW}	Flag for hanging wall sites	1 for sites on the hanging wall (HW) side of the fault, 0 otherwise. The boundary between the foot wall (FW) and HW is defined by the vertical projection of the top of the rupture. For dips of 90 degrees, $F_{HW} = 0$
R_{JB}	Joyner-Boore distance (km)	
R_x	Horizontal distance (km) from top edge of rupture	Measured perpendicular to the fault strike
R_{y0}	Horizontal distance off the end of the rupture measured parallel to strike	Only used for sites on the HW side
Dip	Fault dip in degrees	R_{y0} can only be zero or positive. For sites located along the rupture, $R_{y0} = 0$. Can be computed from $R_{y0} = R_x / \tan(\text{Src2 SiteA}) $
W	Down-dip rupture width (km)	

Based on preliminary regression results, the breaks in the magnitude scaling in Equation 2 are set at $M_2 = 5.0$ and a period-dependent M_1 , ranging between 6.75 at short periods to a maximum of 7.25 at $T = 10$ s.

Style of Faulting (SOF) Model

A preliminary evaluation of the SOF factor found that the difference between ground motions for different faulting style was not seen for the large set of small-magnitude data from California. Therefore, a magnitude-dependent SOF factor was used for both reverse ($RV; f_7$) and normal ($NML; f_8$) earthquakes in which the full scaling is only applied for magnitudes greater than 5 and is tapered to zero effect for magnitude 4 or smaller. The SOF scaling is shown below in Equations 5 and 6:

$$f_7(\mathbf{M}) = \begin{cases} a_{11} & \text{for } \mathbf{M} > 5.0 \\ a_{11}(\mathbf{M} - 4) & \text{for } 4 \leq \mathbf{M} \leq 5 \\ 0 & \text{for } \mathbf{M} < 4.0 \end{cases} \quad (5)$$

$$f_8(\mathbf{M}) = \begin{cases} a_{12} & \text{for } \mathbf{M} > 5.0 \\ a_{12}(\mathbf{M} - 4) & \text{for } 4 \leq \mathbf{M} \leq 5 \\ 0 & \text{for } \mathbf{M} < 4.0 \end{cases} \quad (6)$$

Note that although our functional form allows for scaling of reverse faults, the final regression results are such that there is no scaling between strike-slip and reverse events ($a_{11} = 0$). The scaling of reverse events is instead accounted for by the Z_{TOR} term due to the correlation between SOF and Z_{TOR} in our data set. For large-magnitude events ($\mathbf{M} \geq 5.5$), reverse ruptures tend to be deeper than their equivalent strike slip events.

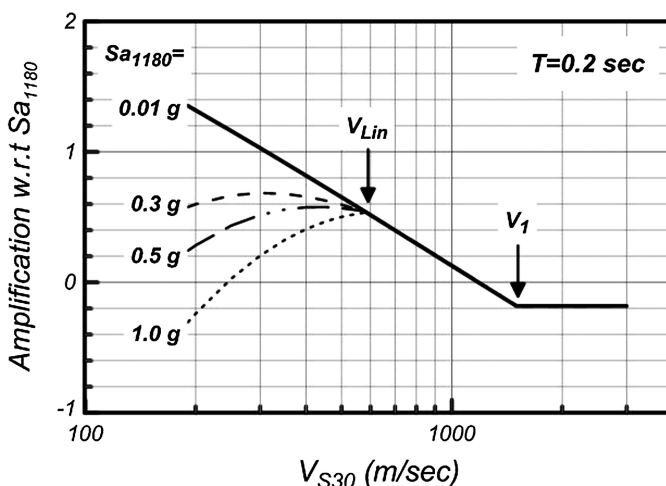


Figure 3. Example of the V_{S30} scaling for $T = 0.2$ s.

Site Response Model

Our model for the V_{S30} dependence of the site amplification is the same as the AS08 form, but uses the median spectral acceleration on hard rock (\widehat{Sa}_{1180}) instead of the peak acceleration to define the strength of shaking. We adopted the nonlinear site response developed by [Kamai et al. \(2014\)](#) using the peninsular range soil model:

Table 3. Constraints on the model parameters

Step	Data set	Estimated parameters	Parameters smoothed after run
1a	$\mathbf{M} > 5.5, R_{RUP} < 80$ km (PGA only)	$a1, a2, a3, a4, a5, a10, a11,$ $a12, a13, a14, a15$	$a4$ (linear mag, $\mathbf{M} 5\text{--}6.75$) $a5$ (linear mag, $\mathbf{M} > 7.75$)
1b	$\mathbf{M} > 5.5, R_{RUP} < 80$ km (HW data only)	$a1, a2, a3, a10, a11, a12, a13,$ $a14, a15$	$a13$ (HW)
1c	$\mathbf{M} > 5.5, R_{RUP} < 80$ km	$a1, a2, a3, a6, a8, a10, a11,$ $a12, a14, a15$	$c4$ (fictitious depth) $a3$ (mag dep GS)
1d	$\mathbf{M} > 4.5, R_{RUP} < 80$ km	$a1, a2, a6, a8, a10, a11, a12,$ $a14, a15, a31$	$a15$ (Z_{TOR}), $a8$ (quadratic magnitude)
1e	$\mathbf{M} > 4.5, R_{RUP} < 80$ km	$a1, a2, a6, a10, a11, a12,$ $a14, a31$	$a11$ (RV SOF) $a12$ (NML SOF) $a14$ (eqk class)
1f	$\mathbf{M} > 4.5, R_{RUP} < 80$ km	$a1, a2, a6, a10, a25, a29, a31,$ $a36, a37, a38, a40, a41, a42$	$a10$ (linear site)
2a	$\mathbf{M} > 4.5$ $R_{RUP} < 300$ (CA, Japan, Taiwan) $R_{RUP} < 80$ (other)	$a1, a2, a6, a17, a25, a29, a31,$ $a36, a37, a38, a40, a41, a42,$ $a43, a44, a45, a46$	$a17$ (linear R)
2b	$\mathbf{M} > 4.5$ $R_{RUP} < 300$ (CA, Japan, Taiwan) $R_{RUP} < 80$ (other)	$a1, a2, a6, a25, a29, a31, a36,$ $a37, a38, a40, a41, a42, a43,$ $a44, a45, a46$	$a2, a43, a44, a45, a46$ (Z1 for V_{S30} bins)
3a	$\mathbf{M} > 3.0$ $R_{RUP} < 300$ (CA, Japan, Taiwan) $R_{RUP} < 80$ (other)	$a1, a6, a25, a29, a31, a36,$ $a37, a38, a40, a41, a42$	$a6$ (small mag linear)
3b	$\mathbf{M} > 3.0$ $R_{RUP} < 300$ (CA, Japan, Taiwan) $R_{RUP} < 80$ (other)	$a1, a25, a29, a31, a36, a37,$ $a38, a40, a41, a42$	$a1$

$$f_5(\widehat{Sa}_{1180}, V_{S30})$$

$$= \begin{cases} (a_{10} + bn) \ln\left(\frac{V_{S30}^*}{V_{Lin}}\right) & \text{for } V_{S30} \geq V_{Lin} \\ (a_{10}) \ln\left(\frac{V_{S30}^*}{V_{Lin}}\right) - b \ln(\widehat{Sa}_{1180} + c) + b \ln\left(\widehat{Sa}_{1180} + c\left(\frac{V_{S30}^*}{V_{Lin}}\right)^n\right) & \text{for } V_{S30} < V_{Lin} \end{cases} \quad (7)$$

where

$$V_{S30}^* = \begin{cases} V_{S30} & \text{for } V_{S30} < V_1 \\ V_1 & \text{for } V_{S30} \geq V_1 \end{cases} \quad (8)$$

The model for the nonlinear site response was selected so that it becomes proportional to $\ln(V_{S30})$ as the input motion (\widehat{Sa}_{1180}) becomes small and as the V_{S30} approaches V_{Lin} . We define another limiting shear-wave velocity term, V_1 , above which there is no scaling with V_{S30} . An example of the relation of the V_{Lin} and V_1 parameters to the site response scaling is shown in Figure 3. For $V_{S30} > V_{Lin}$, there is no dependence on \widehat{Sa}_{1180} , for $V_{S30} > V_1$, there is no dependence on V_{S30} .

To constrain the V_1 term, non-parametric models of the V_{S30} scaling are used (see Abrahamson et al. 2013). At long periods, the scaling with V_{S30} becomes weaker for higher V_{S30} values. This indicates that for rock sites, the V_{S30} is not well correlated with deeper structure that controls the long-period amplification. The following model is used for the period dependence of V_1 :

$$V_1 = \begin{cases} 1500 & \text{for } T \leq 0.5 \text{ s} \\ \exp(-0.35 \ln(\frac{T}{0.5}) + \ln(1500)) & \text{for } 0.5 \text{ s} < T < 3 \text{ s} \\ 800 & \text{for } T \geq 3 \text{ s} \end{cases} \quad (9)$$

The nonlinear site response terms (b, c, n, V_{Lin}) were constrained by the results of the 1-D analytical site response model using the Peninsula Range soil model, as presented in Kamai et al. (2014), with one exception: the b parameter is not allowed to become positive at long periods and is instead constrained to be negative or zero.

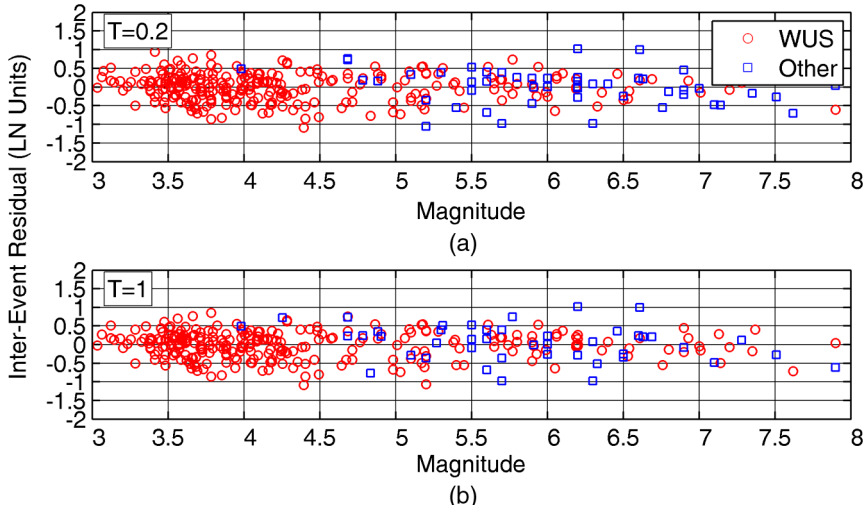


Figure 4. Inter-event residuals for (a) $T = 0.2$ s and (b) $T = 1.0$ s.

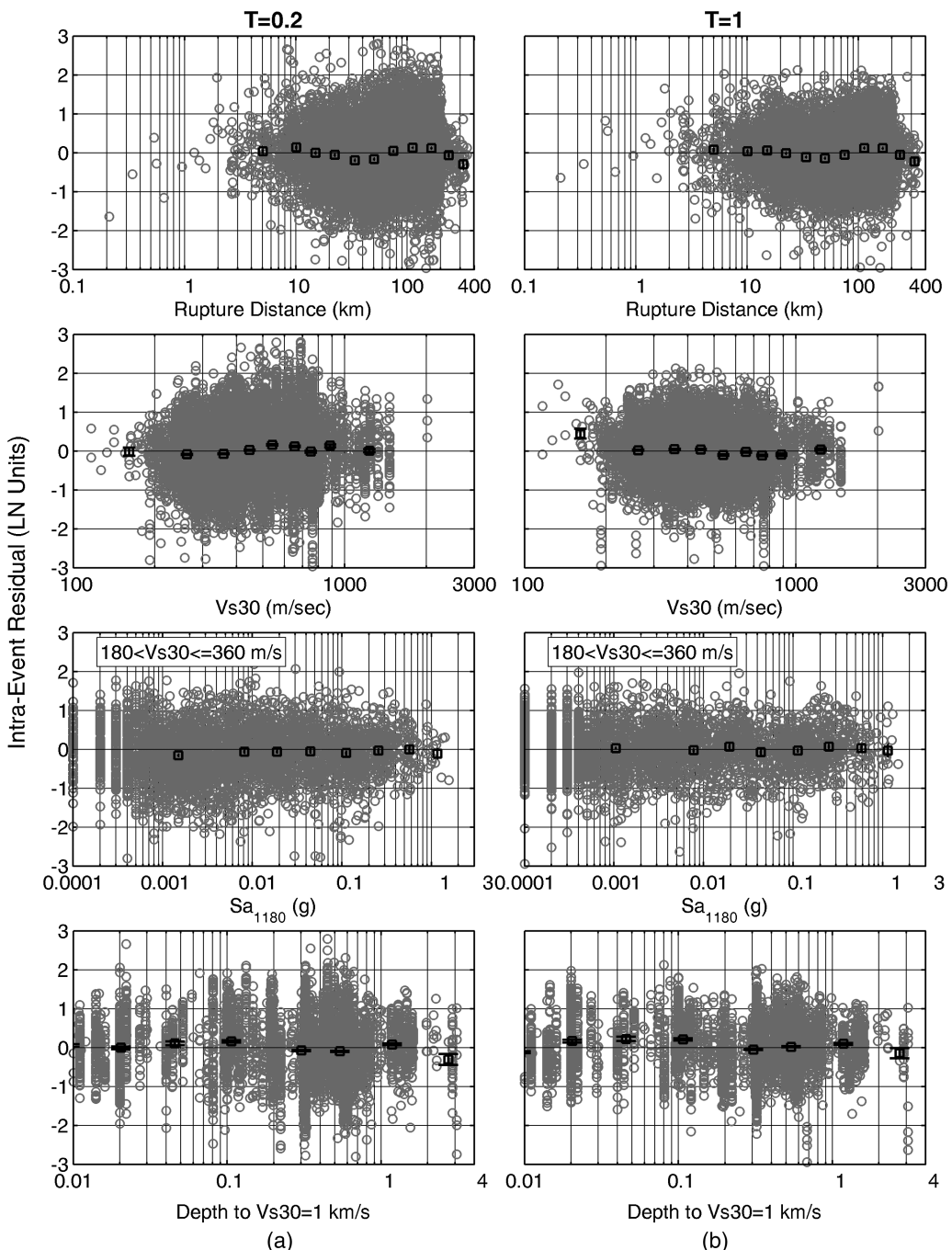


Figure 5. Intra-event residuals of the base model (not including Japan, China, and Taiwan) for (a) $T = 0.2$ s and (b) $T = 1.0$ s.

Table 4. (a) Coefficients for the median ground motion

Parameter	c_4	M_1	M_2	a_1	a_2	a_3	a_4	a_5	a_6	a_8
PGA	4.5	6.75	5	0.587	-0.790	0.275	-0.1	-0.41	2.154	-0.015
PGV	4.5	6.75	5	5.975	-0.919	0.275	-0.1	-0.41	2.366	-0.094
$T = 0.010$	4.5	6.75	5	0.587	-0.790	0.275	-0.1	-0.41	2.154	-0.015
$T = 0.020$	4.5	6.75	5	0.598	-0.790	0.275	-0.1	-0.41	2.146	-0.015
$T = 0.030$	4.5	6.75	5	0.602	-0.790	0.275	-0.1	-0.41	2.157	-0.015
$T = 0.050$	4.5	6.75	5	0.707	-0.790	0.275	-0.1	-0.41	2.085	-0.015
$T = 0.075$	4.5	6.75	5	0.973	-0.790	0.275	-0.1	-0.41	2.029	-0.015
$T = 0.100$	4.5	6.75	5	1.169	-0.790	0.275	-0.1	-0.41	2.041	-0.015
$T = 0.150$	4.5	6.75	5	1.442	-0.790	0.275	-0.1	-0.41	2.121	-0.022
$T = 0.200$	4.5	6.75	5	1.637	-0.790	0.275	-0.1	-0.41	2.224	-0.03
$T = 0.250$	4.5	6.75	5	1.701	-0.790	0.275	-0.1	-0.41	2.312	-0.038
$T = 0.300$	4.5	6.75	5	1.712	-0.790	0.275	-0.1	-0.41	2.338	-0.045
$T = 0.400$	4.5	6.75	5	1.662	-0.790	0.275	-0.1	-0.41	2.469	-0.055
$T = 0.500$	4.5	6.75	5	1.571	-0.790	0.275	-0.1	-0.41	2.559	-0.065
$T = 0.750$	4.5	6.75	5	1.299	-0.790	0.275	-0.1	-0.41	2.682	-0.095
$T = 1.000$	4.5	6.75	5	1.043	-0.790	0.275	-0.1	-0.41	2.763	-0.11
$T = 1.500$	4.5	6.75	5	0.665	-0.790	0.275	-0.1	-0.41	2.836	-0.124
$T = 2.000$	4.5	6.75	5	0.329	-0.790	0.275	-0.1	-0.41	2.897	-0.138
$T = 3.000$	4.5	6.82	5	-0.060	-0.790	0.275	-0.1	-0.41	2.906	-0.172
$T = 4.000$	4.5	6.92	5	-0.299	-0.790	0.275	-0.1	-0.41	2.889	-0.197
$T = 5.000$	4.5	7	5	-0.562	-0.765	0.275	-0.1	-0.41	2.898	-0.218
$T = 6.000$	4.5	7.06	5	-0.875	-0.711	0.275	-0.1	-0.41	2.896	-0.235
$T = 7.500$	4.5	7.15	5	-1.303	-0.634	0.275	-0.1	-0.41	2.870	-0.255
$T = 10.000$	4.5	7.25	5	-1.928	-0.529	0.275	-0.1	-0.41	2.843	-0.285

(b) Coefficients for the median ground motion

Parameter	a_{11}	a_{12}	a_{13}	a_{14}	a_{15}	a_{17}
PGA	0	-0.1	0.6	-0.3	1.1	-0.0072
PGV	0	-0.1	0.25	0.22	0.3	-0.0005
$T = 0.010$	0	-0.1	0.6	-0.3	1.1	-0.0072
$T = 0.020$	0	-0.1	0.6	-0.3	1.1	-0.0073
$T = 0.030$	0	-0.1	0.6	-0.3	1.1	-0.0075
$T = 0.050$	0	-0.1	0.6	-0.3	1.1	-0.0080
$T = 0.075$	0	-0.1	0.6	-0.3	1.1	-0.0089
$T = 0.100$	0	-0.1	0.6	-0.3	1.1	-0.0095
$T = 0.150$	0	-0.1	0.6	-0.3	1.1	-0.0095
$T = 0.200$	0	-0.1	0.6	-0.3	1.1	-0.0086
$T = 0.250$	0	-0.1	0.6	-0.24	1.1	-0.0074
$T = 0.300$	0	-0.1	0.6	-0.19	1.03	-0.0064
$T = 0.400$	0	-0.1	0.58	-0.11	0.92	-0.0043
$T = 0.500$	0	-0.1	0.56	-0.04	0.84	-0.0032

(continued)

Table 4. (*continued*)

Parameter	a_{11}	a_{12}	a_{13}	a_{14}	a_{15}	a_{17}
$T = 0.750$	0	-0.1	0.53	0.07	0.68	-0.0025
$T = 1.000$	0	-0.1	0.5	0.15	0.57	-0.0025
$T = 1.500$	0	-0.1	0.42	0.27	0.42	-0.0022
$T = 2.000$	0	-0.1	0.35	0.35	0.31	-0.0019
$T = 3.000$	0	-0.1	0.2	0.46	0.16	-0.0015
$T = 4.000$	0	-0.1	0	0.54	0.05	-0.0010
$T = 5.000$	0	-0.1	0	0.61	-0.04	-0.0010
$T = 6.000$	0	-0.2	0	0.65	-0.11	-0.0010
$T = 7.500$	0	-0.2	0	0.72	-0.19	-0.0010
$T = 10.000$	0	-0.2	0	0.8	-0.3	-0.0010

(c) Coefficients for the linear and nonlinear soil response

Parameter	a_{10}	V_{Lin}	b	n	c
PGA	1.735	660	-1.47	1.5	2.4
PGV	2.360	330	-2.02	1.5	2400
$T = 0.010$	1.735	660	-1.47	1.5	2.4
$T = 0.020$	1.718	680	-1.459	1.5	2.4
$T = 0.030$	1.615	770	-1.39	1.5	2.4
$T = 0.050$	1.358	915	-1.219	1.5	2.4
$T = 0.075$	1.258	960	-1.152	1.5	2.4
$T = 0.100$	1.310	910	-1.23	1.5	2.4
$T = 0.150$	1.660	740	-1.587	1.5	2.4
$T = 0.200$	2.220	590	-2.012	1.5	2.4
$T = 0.250$	2.770	495	-2.411	1.5	2.4
$T = 0.300$	3.250	430	-2.757	1.5	2.4
$T = 0.400$	3.990	360	-3.278	1.5	2.4
$T = 0.500$	4.450	340	-3.599	1.5	2.4
$T = 0.750$	4.750	330	-3.8	1.5	2.4
$T = 1.000$	4.300	330	-3.5	1.5	2.4
$T = 1.500$	2.600	330	-2.4	1.5	2.4
$T = 2.000$	0.550	330	-1	1.5	2.4
$T = 3.000$	-0.950	330	0	1.5	2.4
$T = 4.000$	-0.950	330	0	1.5	2.4
$T = 5.000$	-0.930	330	0	1.5	2.4
$T = 6.000$	-0.910	330	0	1.5	2.4
$T = 7.500$	-0.870	330	0	1.5	2.4
$T = 10.000$	-0.800	330	0	1.5	2.4

(continued)

Table 4. (d) Coefficients for the Z_1 scaling of the median ground motion

Parameter	a_{43}	a_{44}	a_{45}	a_{46}
PGA	0.1	0.05	0	-0.05
PGV	0.28	0.15	0.09	0.07
$T = 0.010$	0.1	0.05	0	-0.05
$T = 0.020$	0.1	0.05	0	-0.05
$T = 0.030$	0.1	0.05	0	-0.05
$T = 0.050$	0.1	0.05	0	-0.05
$T = 0.075$	0.1	0.05	0	-0.05
$T = 0.100$	0.1	0.05	0	-0.05
$T = 0.150$	0.1	0.05	0	-0.05
$T = 0.200$	0.1	0.05	0	-0.03
$T = 0.250$	0.1	0.05	0	0
$T = 0.300$	0.1	0.05	0.03	0.03
$T = 0.400$	0.1	0.07	0.06	0.06
$T = 0.500$	0.1	0.1	0.1	0.09
$T = 0.750$	0.14	0.14	0.14	0.13
$T = 1.000$	0.17	0.17	0.17	0.14
$T = 1.500$	0.22	0.21	0.2	0.16
$T = 2.000$	0.26	0.25	0.22	0.16
$T = 3.000$	0.34	0.3	0.23	0.16
$T = 4.000$	0.41	0.32	0.23	0.14
$T = 5.000$	0.51	0.32	0.22	0.13
$T = 6.000$	0.55	0.32	0.2	0.1
$T = 7.500$	0.49	0.275	0.17	0.09
$T = 10.000$	0.42	0.22	0.14	0.08

Finally, note that the Kamai et al. model is constrained by the simulation results for $190 \leq V_{S30} \leq 900$ m/s, but can be reasonably extrapolated down to 180 m/s. Consequently, we define our model to be applicable for $180 \leq V_{S30}$. Note that the use of a nonlinear model in our GMPE is not intended to replace site-specific site-response analysis for sites in which nonlinear effects are expected to be significant, but rather to allow the soil sites in our database to be incorporated into the derivation of a GMPE so that nonlinear soil effects are not mapped into magnitude or distance or hanging wall effects.

Hanging Wall Model

Our 2008 model included a HW factor, but the scaling with magnitude and distance were not well constrained. [Donahue and Abrahamson \(2014\)](#); noted herein as DA14) used results from finite-fault simulations to constrain the dependence of the HW effects on magnitude, dip, and distance. Following the DA14 model, the HW factor includes a factor a_{13} , and five tapers to produce a smoothly varying HW effect as a function of the dip, magnitude, location over the rupture, depth, and distance off of the ends of the rupture.

$$\begin{aligned}
f_4(R_{JB}, R_{RUP}, R_x, R_{y0}, W, dip, Z_{TOR}, \mathbf{M}) \\
= a_{13} T_1(dip) T_2(\mathbf{M}) T_3(R_x, W, dip) T_4(Z_{TOR}) T_5(R_x, R_{y0} \text{ OR } R_{JB})
\end{aligned} \quad (10)$$

$$T_1(dip) = \begin{cases} (90 - dip)/45 & \text{for } dip > 30 \\ 60/45 & \text{for } dip \leq 30 \end{cases} \quad (11)$$

$$T_2(\mathbf{M}) = \begin{cases} 1 + a_{2HW}(\mathbf{M} - 6.5) & \text{for } \mathbf{M} \geq 6.5 \\ 1 + a_{2HW}(\mathbf{M} - 6.5) - (1 - a_{2HW})(\mathbf{M} - 6.5)^2 & \text{for } 5.5 < \mathbf{M} < 6.5 \\ 0 & \text{for } \mathbf{M} \leq 5.5 \end{cases} \quad (12)$$

$$T_3(R_x, W, dip) = \begin{cases} h_1 + h_2(R_x/R_1) + h_3(R_x/R_1)^2 & \text{for } R_x < R_1 \\ 1 - \left(\frac{R_x - R_1}{R_2 - R_1}\right) & \text{for } R_1 \leq R_x \leq R_2 \\ 0 & \text{for } R_x > R_2 \end{cases} \quad (13)$$

Table 5. Coefficients for the median ground motion for other regions

Parameter	a_{25}	a_{28}	a_{29}	a_{31}
PGA	-0.0015	0.0025	-0.0034	-0.1503
PGV	-0.0001	0.0005	-0.0037	-0.1462
$T = 0.010$	-0.0015	0.0025	-0.0034	-0.1503
$T = 0.020$	-0.0015	0.0024	-0.0033	-0.1479
$T = 0.030$	-0.0016	0.0023	-0.0034	-0.1447
$T = 0.050$	-0.0020	0.0027	-0.0033	-0.1326
$T = 0.075$	-0.0027	0.0032	-0.0029	-0.1353
$T = 0.100$	-0.0033	0.0036	-0.0025	-0.1128
$T = 0.150$	-0.0035	0.0033	-0.0025	0.0383
$T = 0.200$	-0.0033	0.0027	-0.0031	0.0775
$T = 0.250$	-0.0029	0.0024	-0.0036	0.0741
$T = 0.300$	-0.0027	0.0020	-0.0039	0.2548
$T = 0.400$	-0.0023	0.0010	-0.0048	0.2136
$T = 0.500$	-0.0020	0.0008	-0.0050	0.1542
$T = 0.750$	-0.0010	0.0007	-0.0041	0.0787
$T = 1.000$	-0.0005	0.0007	-0.0032	0.0476
$T = 1.500$	-0.0004	0.0006	-0.0020	-0.0163
$T = 2.000$	-0.0002	0.0003	-0.0017	-0.1203
$T = 3.000$	0	0	-0.0020	-0.2719
$T = 4.000$	0	0	-0.0020	-0.2958
$T = 5.000$	0	0	-0.0020	-0.2718
$T = 6.000$	0	0	-0.0020	-0.2517
$T = 7.500$	0	0	-0.0020	-0.1400
$T = 10.000$	0	0	-0.0020	-0.0216

$$T_4(Z_{TOR}) = \begin{cases} 1 - \frac{Z_{TOR}^2}{100} & \text{for } Z_{TOR} \leq 10 \text{ km} \\ 0 & \text{for } Z_{TOR} > 10 \text{ km} \end{cases} \quad (14)$$

$$T_5(R_x, R_{y0}) = \begin{cases} 1 & \text{for } R_{y0} - R_{y1} \leq 0 \\ 1 - \frac{R_{y0} - R_{y1}}{5} & \text{for } 0 < R_{y0} - R_{y1} < 5 \\ 0 & \text{for } R_{y0} - R_{y1} \geq 5 \end{cases} \quad (15a)$$

where $R_1 = W \cos(dip)$, $R_2 = 3R_1$, $R_{y1} = R_x \tan(20)$, $h_1 = 0.25$, $h_2 = 1.5$ and $h_3 = -0.75$.

R_{y0} is a new parameter that can be computed from $R_{y0} = R_x / |\tan(\text{Src2SiteA})|$. It can only be zero (for sites located along the rupture) or positive. If the R_{y0} distance metric is not available, the T_5 taper can be replaced using the following model:

$$T_5(R_{JB}) = \begin{cases} 1 & \text{for } R_{JB} = 0 \\ 1 - \frac{R_{JB}}{30} & \text{for } R_{JB} < 30 \\ 0 & \text{for } R_{JB} \geq 30 \end{cases} \quad (15b)$$

Table 6. Coefficients for the V_{S30} scaling of the median ground motion for Japan

Parameter	a_{36}	a_{37}	a_{38}	a_{39}	a_{40}	a_{41}	a_{42}
PGA	0.265	0.337	0.188	0	0.088	-0.196	0.044
PGV	0.377	0.212	0.157	0	0.095	-0.038	0.065
$T = 0.010$	0.265	0.337	0.188	0	0.088	-0.196	0.044
$T = 0.020$	0.255	0.328	0.184	0	0.088	-0.194	0.061
$T = 0.030$	0.249	0.320	0.180	0	0.093	-0.175	0.162
$T = 0.050$	0.202	0.289	0.167	0	0.133	-0.090	0.451
$T = 0.075$	0.126	0.275	0.173	0	0.186	0.090	0.506
$T = 0.100$	0.022	0.256	0.189	0	0.160	0.006	0.335
$T = 0.150$	-0.136	0.162	0.108	0	0.068	-0.156	-0.084
$T = 0.200$	-0.078	0.224	0.115	0	0.048	-0.274	-0.178
$T = 0.250$	0.037	0.248	0.122	0	0.055	-0.248	-0.187
$T = 0.300$	-0.091	0.203	0.096	0	0.073	-0.203	-0.159
$T = 0.400$	0.129	0.232	0.123	0	0.143	-0.154	-0.023
$T = 0.500$	0.310	0.252	0.134	0	0.160	-0.159	-0.029
$T = 0.750$	0.505	0.208	0.129	0	0.158	-0.141	0.061
$T = 1.000$	0.358	0.208	0.152	0	0.145	-0.144	0.062
$T = 1.500$	0.131	0.108	0.118	0	0.131	-0.126	0.037
$T = 2.000$	0.123	0.068	0.119	0	0.083	-0.075	-0.143
$T = 3.000$	0.109	-0.023	0.093	0	0.070	-0.021	-0.028
$T = 4.000$	0.135	0.028	0.084	0	0.101	0.072	-0.097
$T = 5.000$	0.189	0.031	0.058	0	0.095	0.205	0.015
$T = 6.000$	0.215	0.024	0.065	0	0.133	0.285	0.104
$T = 7.500$	0.150	-0.070	0.000	0	0.151	0.329	0.299
$T = 10.000$	0.092	-0.159	-0.050	0	0.124	0.301	0.243

The first three tapers (T_1 , T_2 , and T_3) are constrained by the DA14 model but include some modifications. For the magnitude taper (T_2), we smoothed the a_{2HW} term in the DA14 model to be 0.2 for all periods. For the distance tapers (T_3 and T_5), the values of h_1 , h_2 , and h_3 are set by DA14 while the models for R_2 and R_{y1} were set based on an evaluation of the HW residuals from the Chi-Chi data, which has the largest number of hanging wall recordings. There were only two Z_{TOR} values considered in the DA14 model ($Z_{TOR} = 0$ km and $Z_{TOR} = 5$ km), so this model did not provide constraints on the HW scaling with Z_{TOR} for depths greater than 5 km. We assumed that the HW effect reduced to zero at $Z_{TOR} = 10$ km. Finally, the scaling off the end of the rupture (T_5) found in the DA14 model showed the HW effect remaining for much larger R_x distances than seen in the empirical data. Although the empirical data is sparse, we relied on the empirical data from the Chi-Chi, Taiwan, earthquake to set this scaling.

Although a complex form is used such that the HW effect scales in a reasonable manner with magnitude, dip, depth, and distance, only the a_{13} term (e.g., maximum amplitude of HW effect for $M = 6.5$, dip = 45, $Z_{TOR} = 0$) was estimated in the regression analysis (see Table 3).

Table 7. Coefficients for the standard deviation

Parameter	V_{S30} estimated		V_{S30} measured		Japan			
	s_1	s_2	s_1	s_2	s_3	s_4	s_5	s_6
PGA	0.754	0.520	0.741	0.501	0.47	0.36	0.54	0.63
PGV	0.662	0.510	0.660	0.510	0.38	0.38	0.58	0.53
0.010	0.754	0.520	0.741	0.501	0.47	0.36	0.54	0.63
0.020	0.760	0.520	0.747	0.501	0.47	0.36	0.54	0.63
0.030	0.781	0.520	0.769	0.501	0.47	0.36	0.55	0.63
0.050	0.810	0.530	0.798	0.512	0.47	0.36	0.56	0.65
0.075	0.810	0.540	0.798	0.522	0.47	0.36	0.57	0.69
0.100	0.810	0.550	0.795	0.527	0.47	0.36	0.57	0.7
0.150	0.801	0.560	0.773	0.519	0.47	0.36	0.58	0.7
0.200	0.789	0.565	0.753	0.514	0.47	0.36	0.59	0.7
0.250	0.770	0.570	0.729	0.513	0.47	0.36	0.61	0.7
0.300	0.740	0.580	0.693	0.519	0.47	0.36	0.63	0.7
0.400	0.699	0.590	0.644	0.524	0.47	0.36	0.66	0.7
0.500	0.676	0.600	0.616	0.532	0.47	0.36	0.69	0.7
0.750	0.631	0.615	0.566	0.548	0.47	0.36	0.73	0.69
1.000	0.609	0.630	0.541	0.565	0.47	0.36	0.77	0.68
1.500	0.578	0.640	0.506	0.576	0.47	0.36	0.80	0.66
2.000	0.555	0.650	0.480	0.587	0.47	0.36	0.80	0.62
3.000	0.548	0.640	0.472	0.576	0.47	0.36	0.80	0.55
4.000	0.527	0.630	0.447	0.565	0.47	0.36	0.76	0.52
5.000	0.505	0.630	0.425	0.568	0.47	0.36	0.72	0.5
6.000	0.477	0.630	0.395	0.571	0.47	0.36	0.70	0.5
7.500	0.457	0.630	0.378	0.575	0.47	0.36	0.67	0.5
10.000	0.429	0.630	0.359	0.585	0.47	0.36	0.64	0.5

Depth-to-Top of Rupture Model

We find that buried ruptures are on average more energetic than events that rupture to the surface, and hence, we parameterize that with Z_{TOR} , the vertical depth to the shallowest point on the rupture surface. Based on preliminary evaluations, we simplified the AS08 model to use the same depth scaling for all styles of faulting. Although there is some evidence for a reduction of the depth dependence at shallow depths, we used a linear scaling at all depths for simplicity. To avoid having the small-magnitude data control the scaling for the large magnitudes, the scaling was constrained in Step 1 of the regression for $M > 4.5$ (see Table 3). There is still sparse data at large Z_{TOR} values (greater than 20 km). To avoid an unconstrained extrapolation, the depth scaling is capped at 20 km depth.

$$f_6(Z_{TOR}) = \begin{cases} a_{15} \frac{Z_{TOR}}{20} & \text{for } Z_{TOR} < 20 \text{ km} \\ a_{15} & \text{for } Z_{TOR} \geq 20 \text{ km} \end{cases} \quad (16)$$

Soil Depth Model

Scaling with respect to sediment thickness is parameterized in our model by the depth to the shear wave velocity horizon of 1.0 km/s, Z_1 . In the AS08 model, we used results from analytical modeling (both three-dimensional, or 3-D, basin modeling and 1-D shallow site response modeling) to constrain the soil depth scaling due to the sparse and sometimes inconsistent Z_1 values in the 2008 NGA data set. In the NGA-West2 data set, there are many more sites with Z_1 values. Therefore, we used the empirical data to set the Z_1 scaling. Of the 15,750 recordings in our selected data set, 9,668 have estimates of Z_1 . For the remaining 6,082 recordings without Z_1 estimates, we set $Z_1 = Z_{1,ref}(V_{S30})$, where $Z_{1,ref}$ is the average Z_1 for the given V_{S30} value.

Preliminary evaluations showed that the Z_1 scaling is dependent on the V_{S30} value. We used a non-parametric approach to model this dependence by using V_{S30} bins:

$$f_{10}(Z_1, V_{S30}) = \begin{cases} a_{43} \ln\left(\frac{Z_1+0.01}{Z_{1,ref}+0.01}\right) & \text{for } V_{S30} \leq 200 \\ a_{44} \ln\left(\frac{Z_1+0.01}{Z_{1,ref}+0.01}\right) & \text{for } 200 < V_{S30} \leq 300 \\ a_{45} \ln\left(\frac{Z_1+0.01}{Z_{1,ref}+0.01}\right) & \text{for } 300 < V_{S30} \leq 500 \\ a_{46} \ln\left(\frac{Z_1+0.01}{Z_{1,ref}+0.01}\right) & \text{for } 500 < V_{S30} \end{cases} \quad (17)$$

A smooth model is recommended for application, as described in the section “application guidelines.” For the reference Z_1 value, we adopted the preliminary relationships developed by [Chiou and Youngs \(2014\)](#) for Z_1 (in km) as a function of V_{S30} . The relationships for California and Japan are shown in Equations 18 and 19, respectively:

$$Z_{1,ref} = \frac{1}{1000} \exp\left(-\frac{7.67}{4} \ln\left(\frac{V_{S30}^4 + 610^4}{1360^4 + 610^4}\right)\right) \quad (18)$$

$$Z_{1,ref} = \frac{1}{1000} \exp\left(-\frac{5.23}{2} \ln\left(\frac{V_{S30}^2 + 412^2}{1360^2 + 412^2}\right)\right) \quad (19)$$

Aftershock Scaling

Previous studies, such as AS08, have found that the median short-period ground motions from aftershocks are smaller than the median ground motions from main shocks. The definition for aftershocks has been modified in the NGA-West2 project, using the definition of Class 1 and Class 2 events as described in [Wooddell and Abrahamson \(2014\)](#). They define a new distance classification, called the Centroid Joyner-Boore distance, or CR_{JB} , which is the shortest distance between the centroid of Joyner-Boore rupture surface of the potential Class 2 earthquakes and the closest point on the edge of the Joyner-Boore rupture surface of the main shock. According to this new terminology, we define Class 2 events as those events that have a $CR_{JB} < 15$ km and that fall within the [Gardner and Knopoff \(1974\)](#) time window. Following the hypothesis that the stress drops are lower for earthquakes that re-rupture the Class 1 main shock rupture plane, the ground motions from Class 2 events are scaled using the following expression:

$$f_{11}(CR_{JB}) = \begin{cases} a_{14} & \text{for } CR_{JB} \leq 5 \\ 1 - \frac{a_{14}}{10} & \text{for } 5 < CR_{JB} < 15 \\ 0 & \text{for } CR_{JB} \geq 15 \end{cases} \quad (20)$$

Regionalization

We allowed for regionalization of the V_{S30} scaling and the anelastic attenuation (i.e., Q term) for the data from Taiwan, Japan, and China. In all cases, the additional coefficient is added to the base model (all other regions, dominated by California), which is used as a reference. For all three regions, we allow for a difference in the large-distance (linear R) terms, such that the linear R coefficients a_{25} for Taiwan, a_{28} for China, and a_{29} for Japan, are added to the base model coefficient, a_{17} . The regionalization is given by:

$$\begin{aligned} Regional(V_{S30}, R_{RUP}) = & F_{TW}(f_{12}(V_{S30}) + a_{25}R_{RUP}) + F_{CN}(a_{28}R_{RUP}) \\ & + F_{JP}(f_{13}(V_{S30}) + a_{29}R_{RUP}) \end{aligned} \quad (21)$$

where F_{TW} equals 1.0 for Taiwan and 0 for all other regions, F_{CN} equals 1.0 for China and 0 for all other regions, and F_{JP} equals 1.0 for Japan and 0 for all other regions.

The linear V_{S30} scaling in the base model is described by the coefficients $a_{10} + bn$. For Taiwan, the change in the $\ln(V_{S30})$ slope is included, using the coefficient a_{31} .

$$f_{12}(V_{S30}) = a_{31} \ln\left(\frac{V_{S30}^*}{V_{Lin}}\right) \quad (22)$$

For Japan, the preliminary analyses showed a break in the V_{S30} scaling, such that there is no constant slope for all V_{S30} values. Therefore, for the Japanese data, we allowed for a non-parametric deviation from the base $\ln(V_{S30})$ scaling using V_{S30} bins, expressed by the coefficients a_{36} through a_{42} for the different V_{S30} bins, as follows:

$$f_{13}(V_{S30}) = \begin{cases} a_{36} & \text{for } V_{S30} < 200 \text{ m/s} \\ a_{37} & \text{for } 200 \leq V_{S30} < 300 \text{ m/s} \\ a_{38} & \text{for } 300 \leq V_{S30} < 400 \text{ m/s} \\ a_{39} & \text{for } 400 \leq V_{S30} < 500 \text{ m/s} \\ a_{40} & \text{for } 500 \leq V_{S30} < 700 \text{ m/s} \\ a_{41} & \text{for } 700 \leq V_{S30} < 1000 \text{ m/s} \\ a_{42} & \text{for } V_{S30} \geq 1000 \text{ m/s} \end{cases} \quad (23)$$

A smooth model is recommended for application, as described in the section “application guidelines.” The middle V_{S30} bin $400 \text{ m/s} \leq V_{S30} < 500 \text{ m/s}$ was set as a reference value, and its coefficient (a_{39}) was set to zero to normalize the site amplification relative to the base model. A regionalized V_{S30} scaling for China was not included due to the smaller amount of data available.

Constant Displacement Model

At long spectral periods, the response spectrum for rock sites will reach a constant displacement. The period in which the displacement spectra should become flat (T_D) corresponds to the corner frequency of the Brune point-source spectrum, with larger magnitudes having a longer T_D . In the AS08 model, the spectral displacement was constrained to reach a constant value at long periods. In the new model, a reasonable constant displacement spectrum was obtained by regression alone and such constraint was not required. A near-constant displacement was achieved with minor adjustments, mainly to the coefficient a_8 .

Application Guidelines

The V_{S30} scaling in our GMPE is only applicable if the site-specific V_S profile is within the range of the V_S profiles used for generating the model. The use of V_{S30} to represent the site response should not suggest that it is a fundamental physical parameter for predicting site response. Rather, V_{S30} is an index that is correlated with the deeper profile and thus would be constrained by the data used to generate each of the three regional V_{S30} models (California, Taiwan, and Japan).

Soft soil sites should require a site-specific analysis; the use of a nonlinear model in our GMPE is not intended to replace site-specific site-response analysis, but rather to allow the soil sites in our database to be incorporated into the derivation of a GMPE so that nonlinear soil effects are not mapped into magnitude or distance or hanging wall effects.

For forward applications, the non-parametric components, Z_1 scaling (Equation 17) and Japanese V_{S30} scaling (Equation 23), should be formulated such that the coefficients are placed at the bin centers and linearly interpolated in between.

The full functional form, which will be described below, is coded into Matlab and provided as an electronic supplement to this paper, titled “ASK14.m.” The required list of coefficients in the format read by the code is also provided in the file “ASK14_coeffs.m.”

REGRESSION RESULTS

The random-effects model was used for the regression analysis following the procedure described by [Abrahamson and Youngs \(1992\)](#) with modifications for the effects of the non-linear site response on the standard deviations described in [Al Atik and Abrahamson \(2010\)](#). The random-effects method leads to two types of residuals: inter-event residuals (τ) and intra-event (ϕ) residuals. The effects of nonlinear site response on τ and ϕ are included in the likelihood function.

The regression is performed in a number of steps, starting with a more limited data set and proceeding to the full range, including $M > 3$, $R_{RUP} < 300$ km. Table 3 lists the parameters that were determined through regression in each step and those which were smoothed and fixed following each step. The step numbers are consistent with Figure 2, which shows the number of events and number of recordings for each step.

A key issue we faced was the large-magnitude scaling at long periods ($T = 1$ s to 3 s). In this range, the Wenchuan earthquake ($M 7.9$) has very weak ground motions, which were inconsistent with scaling seen from finite-fault numerical simulations ([Collins et al. 2006](#)). Due to this inconsistency, the Wenchuan earthquake is removed from the early regression steps (Steps 1 and 2) but is included in Step 3 of the regression, once the magnitude scaling is fixed. This allows the Wenchuan data to affect the standard deviation, but not the median in terms of the magnitude scaling.

To arrive at a smooth model, the coefficients were smoothed in a series of steps. The details of this smoothing are described in [Abrahamson et al. \(2013\)](#). The final smoothed coefficients for the median ground motion and for the standard deviation model are listed in an electronic supplement titled “ASK14_coeffs.xls.”

Correlations of the inter-event and intra-event residuals, required for vector hazard and conditional mean spectra are also provided in the electronic supplement titled “ASK14_coeffs.xls.”

RESIDUALS

When performing a random-effects regression, the residuals are separated into inter-event (between events) and intra-event (within event) terms. An extensive set of residual plots is provided in [Abrahamson et al. \(2013\)](#), showing and discussing trends of residuals against many of the model parameters. Due to space limitations, only examples are provided below.

An example of the magnitude dependence of the inter event $T = 0.2$ s and $T = 1.0$ s are shown in Figure 4. The open circles represent the Western United States (WUS) data, while the open squares represent all other regions. No magnitude dependence is apparent.

Examples of the distance, V_{530} , Sa_{1180} , and Z_1 dependence of the intra-event residuals of the base model (not including China, Taiwan, and Japan) are shown in Figure 5 for $T = 0.2$ s and $T = 1.0$ s. The data is binned along the X-axis and bin-medians are shown by the error-bars, so that any trends in the residuals can be clearly seen. These plots show that the model fits the data well and there are no significant trends in the residuals. A complete set of residual plots for a wider range of spectral periods is given in [Abrahamson et al. \(2013\)](#).

EQUATIONS FOR STANDARD DEVIATION

The total standard deviation is computed as $\sqrt{\phi^2 + \tau^2}$, where ϕ and τ are the intra-event and inter-event standard deviations, respectively. The intra-event and inter-event standard deviations are magnitude dependent, as follows:

$$\phi_{A,L}(\mathbf{M}) = \begin{cases} s_1 & \text{for } \mathbf{M} < 4 \\ s_1 + \frac{s_2 - s_1}{2}(\mathbf{M} - 4) & \text{for } 4 \leq \mathbf{M} \leq 6 \\ s_2 & \text{for } \mathbf{M} > 6 \end{cases} \quad (24)$$

and

$$\tau_{A,L}(\mathbf{M}) = \begin{cases} s_3 & \text{for } \mathbf{M} < 5 \\ s_3 + \frac{s_4 - s_3}{2}(\mathbf{M} - 5) & \text{for } 5 \leq \mathbf{M} \leq 7 \\ s_4 & \text{for } \mathbf{M} > 7 \end{cases} \quad (25)$$

The subscript L denotes that these are the linear standard deviation terms, that is, without accounting for the effects of nonlinear site response on the standard deviation. The coefficients s_1 and s_2 are provided separately for an estimated V_{S30} and a measured V_{S30} due to the uncertainty associated with an estimated V_{S30} value (see detailed derivation in [Abrahamson et al. 2013](#)). The smoothed s_1 through s_4 parameters are provided in the electronic supplement titled “ASK14_coeffs.xls” and are presented in Figures 14 and 15.

REGIONALIZATION OF STANDARD DEVIATION

The intra-event standard deviation of the Japanese data is significantly higher than that from California and Taiwan. Therefore, we created a separate model for the Japanese intra-event standard deviation so that it would not affect the results of the other regions. Since our data set includes only five Japanese events, all with magnitudes between 6.0 and 7.0, we cannot determine the magnitude scaling for this data. On the other hand, we see a clear distance scaling for the Japanese standard deviation, which is not apparent for the other regions. Hence, the intra-event standard deviation model for Japan has the following form:

$$\phi_{A,L-JP}(R_{RUP}) = \begin{cases} s_5 & \text{for } R_{RUP} < 30 \\ s_5 + \frac{s_6 - s_5}{50}(R_{RUP} - 30) & \text{for } 30 \leq R_{RUP} \leq 80 \\ s_6 & \text{for } R_{RUP} > 80 \end{cases} \quad (26)$$

NONLINEAR EFFECTS ON THE STANDARD DEVIATION

The standard deviation in the linear site response range is dependent on the earthquake magnitude. The nonlinear site effects also affect the standard deviation and the same approach as used in AS08 is used here with the difference being that the level of shaking is parameterized by the \widehat{Sa}_{1180} instead of the \widehat{PGA}_{1180} .

As discussed in [Al Atik and Abrahamson \(2010\)](#), the nonlinear effects on the standard deviation are influenced by the variability of the rock motion. If the rock motion is above average, the amplification will have more nonlinearity and, as a result, will be below average. Similarly, if the rock motion is below average, the amplification will have less nonlinearity

and hence will be above average. That effect leads to a reduction in the variability in the short-period soil motion.

Because the nonlinear effect depends on the variability of the rock motion, we need to estimate the standard deviation of the rock motion. We can estimate the standard deviation of the rock motion by removing the site amplification variability from the surface motion:

$$\phi_B(\mathbf{M}, T) = \sqrt{\phi_{A,L}^2(\mathbf{M}, T) - \phi_{Amp}^2(T)} \quad (27)$$

where $\phi_{A,L}$ is the linear intra-event standard deviation for soil that is derived from the regression, ϕ_{Amp} is the standard deviation of the site amplification, and ϕ_B is the standard deviation of the rock motion. We assume that $\phi_{Amp}(T) = 0.4$ for all periods based on the site response simulation results described in Kamai et al. (2014). For the inter-event variability, the standard deviation of the rock motion is the observed inter-event variability for the linear range, so $\tau_B(\mathbf{M}, T) = \tau_{A,L}(\mathbf{M}, T)$.

To account for the effects of nonlinearity on the soil ground motion, the variability of the soil motion is computed using propagation of errors. The intra-event standard deviation is given by:

$$\phi(T, \mathbf{M}, \widehat{Sa}_{1180}, V_{S30}) = \left[\phi_B^2(\mathbf{M}, T) \left(1 + \frac{\partial \ln Amp(T, \widehat{Sa}_{1180}, V_{S30})}{\partial \ln Sa_{1180}} \right)^2 + \phi_{Amp}^2(T) \right]^{1/2} \quad (28)$$

and the inter-event standard deviation is given by

$$\tau(T, \mathbf{M}, \widehat{Sa}_{1180}, V_{S30}) = \tau_B(\mathbf{M}, T) \left(1 + \frac{\partial \ln Amp(T, \widehat{Sa}_{1180}, V_{S30})}{\partial \ln Sa_{1180}} \right) \quad (29)$$

where

$$\frac{\partial \ln Amp(T, \widehat{Sa}_{1180}, V_{S30})}{\partial \ln Sa_{1180}} = \begin{cases} 0 & \text{for } V_{S30} \geq V_{Lin} \\ \frac{-b(T)\widehat{Sa}_{1180}}{\widehat{Sa}_{1180}+c} + \frac{b(T)\widehat{Sa}_{1180}}{\widehat{Sa}_{1180}+c\left(\frac{V_{S30}}{V_{Lin}}\right)^n} & \text{for } V_{S30} < V_{Lin} \end{cases} \quad (30)$$

MODEL RESULTS

MEDIAN GROUND MOTION

All plots in this section represent the base model (excluding Taiwan, China, and Japan), unless noted otherwise. The median response spectra for the ASK14 model are compared to the AS08 model in Figures 6a and b for a vertical strike-slip scenario at an R_{JB} distance of 30 km and V_{S30} values of 760 m/s and 270 m/s, respectively. For this case, the Z_{TOR} values are 8, 6.5, 3, and 0 for magnitudes 5, 6, 7, and 8, respectively. The Z_1 values are set at the Z_{ref} value (Chiou and Youngs 2014) for the given V_{S30} . Figure 6 shows that the median spectra from the current model are higher than those from AS08 for large magnitudes at short periods, but lower than those from AS08 for longer periods, especially for smaller magnitudes

(e.g., $M = 5.0$). The difference between the two models is larger for rock sites (Figure 6a) than for soil sites (Figure 6b). A similar comparison of the medians at a R_{JB} distance of 1 km is shown in Figure 7a–b for V_{S30} values of 760 m/s and 270 m/s.

The distance scaling is shown in Figure 8 for PGA and spectral periods of 0.2 s, 1.0 s, and 3.0 s. In this figure, the median ground motion from vertical strike-slip earthquakes on rock

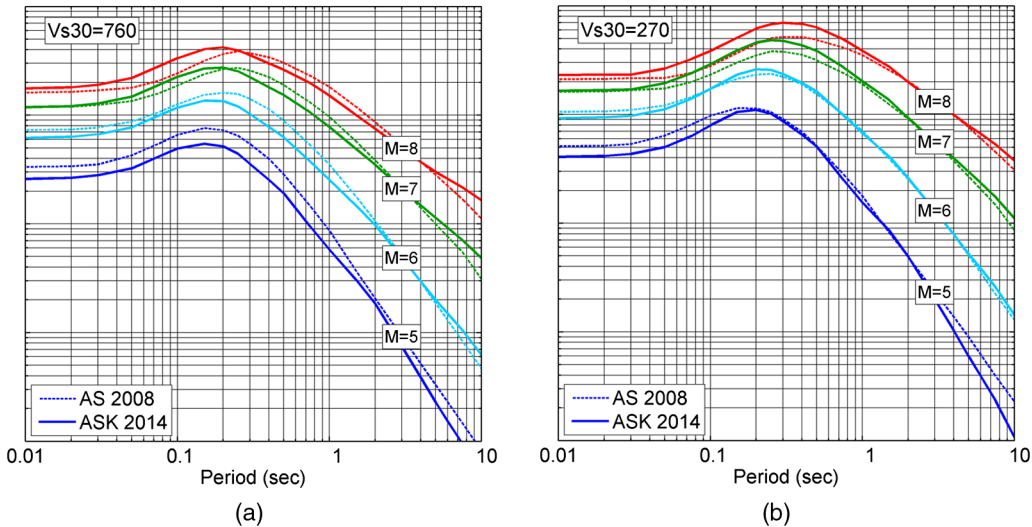


Figure 6. Comparison of the median spectral acceleration from the current model with the median from the AS08 model for vertical strike-slip earthquakes for $R_{JB} = 30$ km. (a) $V_{S30} = 760$ m/s, (b) $V_{S30} = 270$ m/s.

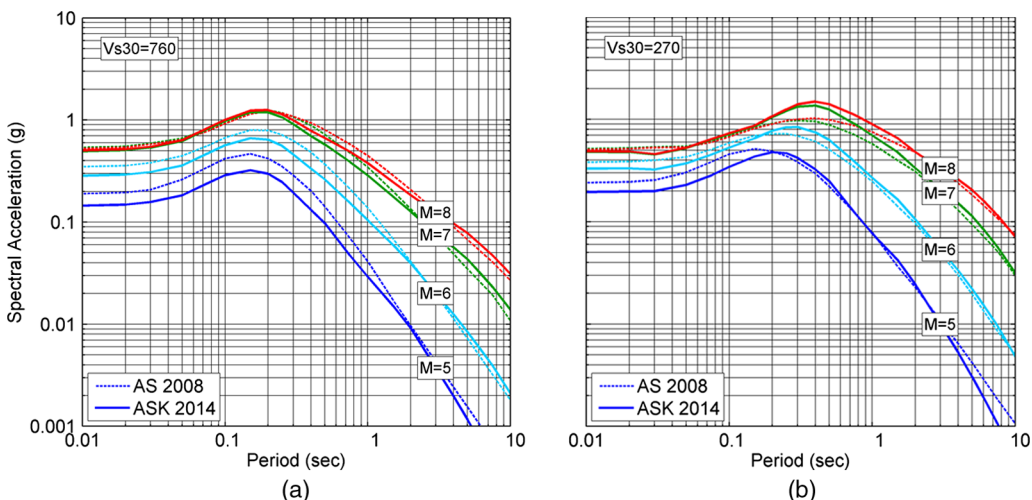


Figure 7. Comparison of the median spectral acceleration from the current model with the median from the AS08 model for vertical strike-slip earthquakes for $R_{JB} = 1$ km. (a) $V_{S30} = 760$ m/s, (b) $V_{S30} = 270$ m/s.

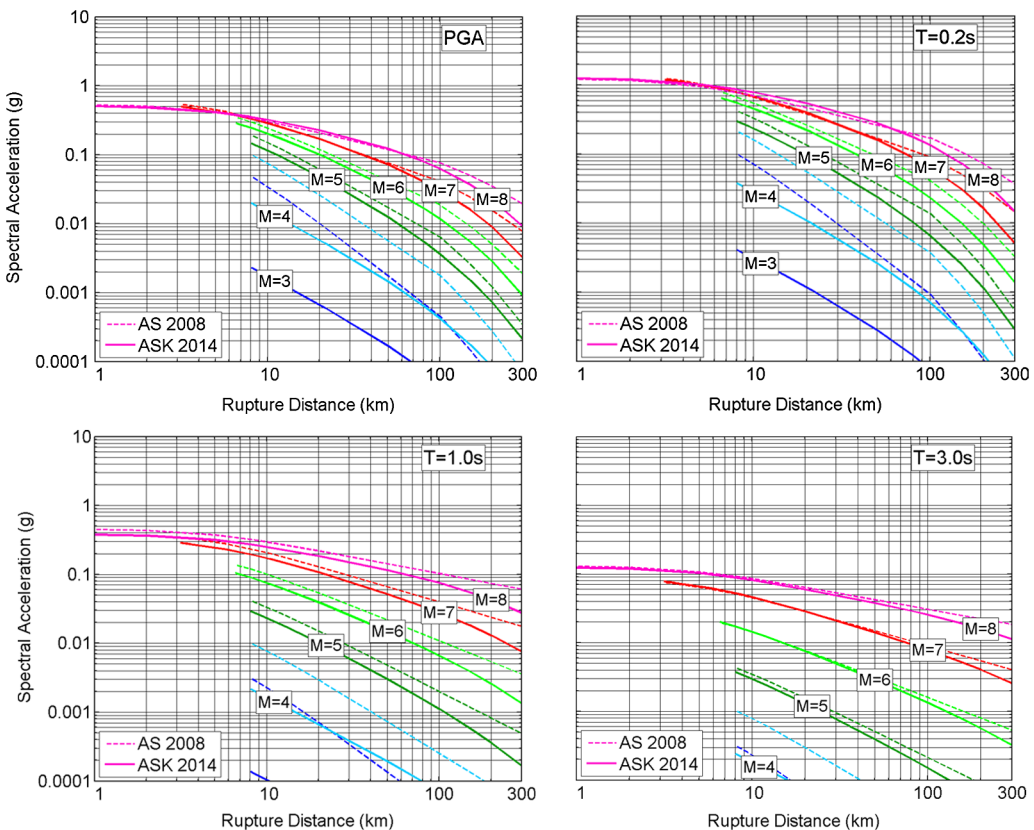


Figure 8. Comparison of the scaling with distance for the current model with the AS08 model for strike-slip earthquakes and rock site conditions ($V_{S30} = 760$ m/s).

site conditions ($V_{S30} = 760$ m/s) is shown for six different magnitudes. A significant reduction in the median ground motion between AS08 to ASK14 can be seen, especially for smaller magnitudes and for large distances. Note that the crossing of the **M** 7.0 and **M** 8.0 curves is due to the Z_{TOR} scaling.

The magnitude scaling of the current model is shown in Figures 9 for vertical strike-slip earthquakes on rock site conditions ($V_{S30} = 760$ m/s) for $T = 0.2$ and $T = 3.0$ s. Note that the break in the magnitude scaling at **M** 5.0 is driven by the additional small-magnitude data set which was not available in 2008, hence the large difference between the models for small magnitudes. The weak scaling of the short-period motion at short distances reflects the saturation with magnitude.

The HW scaling for a reverse **M** 6.7 rupture with 45° dip is shown in Figure 10 for PGA on rock site conditions ($V_{S30} = 760$ m/s). While the AS08 model had a step in the ground motion from the foot wall (FW) to the HW for surface ruptures only, such a step is now present for both surface and buried ruptures, but it is smoother. The HW term is now tapering

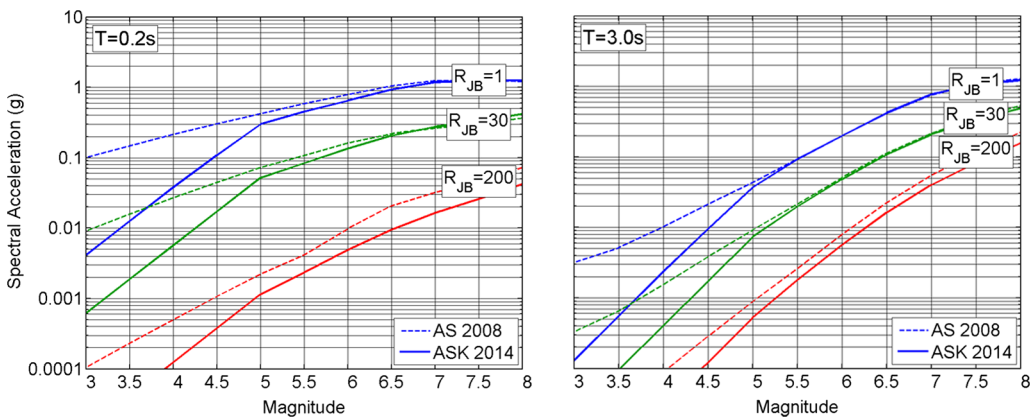


Figure 9. Magnitude scaling for strike-slip earthquakes and rock site condition ($V_{S30} = 760$ m/s) for $T = 0.2$ s and $T = 3$ s.

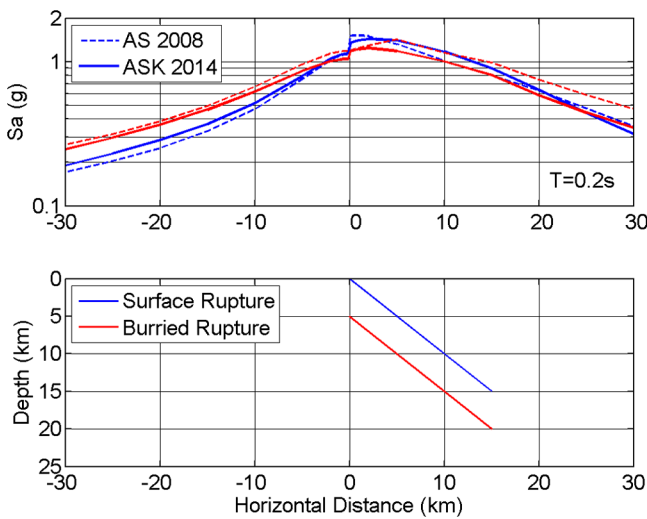


Figure 10. Attenuation of peak acceleration on the HW and FW for M 7, rock ($V_{S30} = 760$ m/s) for buried and surface ruptures. The bottom panel shows a cross section for the surface and buried ruptures.

more smoothly back to the baseline FW value, at a distance away from the down-dip fault edge that depends on the fault dip and width (see Equation 13). The short-period ground motion on the FW is larger for buried ruptures than for surface ruptures, due to the scaling with Z_{TOR} , but on the HW the ground motions for the buried rupture are smaller due to the Z_{TOR} HW taper.

The site response scaling for M 7.0 vertical strike-slip earthquakes at a rupture distance of 30 km is shown in Figures 11 and 12. Figure 11 shows the dependence of the

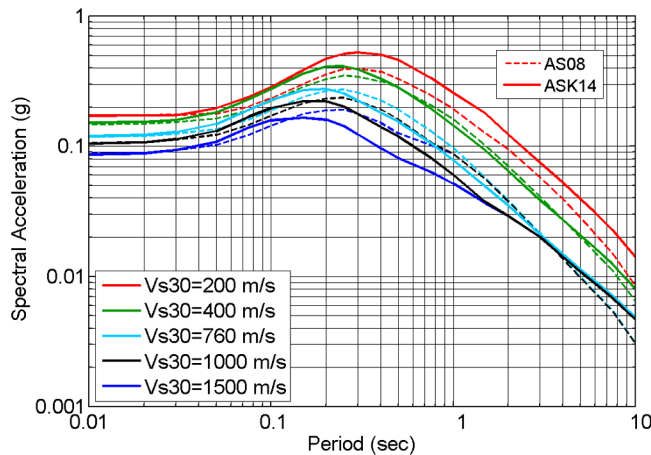


Figure 11. Scaling with V_{S30} for a M 7.0 strike slip event at a rupture distance of 30 km.

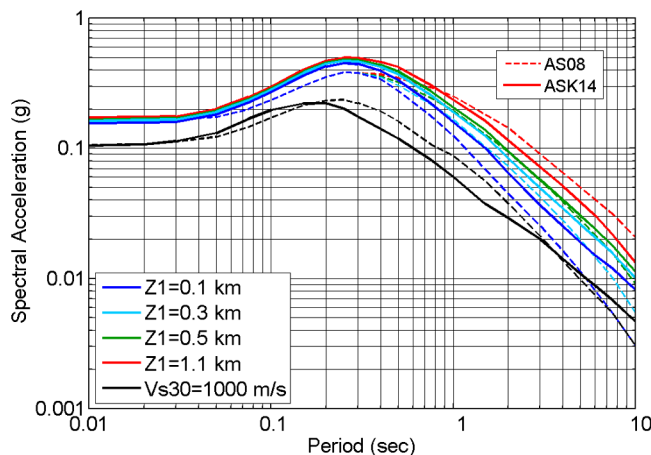


Figure 12. Scaling with soil depth for a M 7.0 strike slip event at a rupture distance of 30 km and $V_{S30} = 270$ m/s.

spectra on V_{S30} , with $Z_1 = Z_{1,\text{ref}}$, as calculated from Equation 18. Figure 12 shows that dependence of the spectra on Z_1 for a soil site with $V_{S30} = 270$ m/s. Note that in Figure 11 the higher velocities taper together at long periods due to the V_1 constraint while in Figure 12 all soil sites taper together at short periods, since the Z_1 scaling only affects periods longer than 0.2 s.

The spectral displacements of a vertical strike slip fault at a R_{JB} distance of 20 km is shown in Figure 13 for a range of magnitudes. Although the spectral displacement was not constrained to a constant value at long periods for this model, the regression leads to

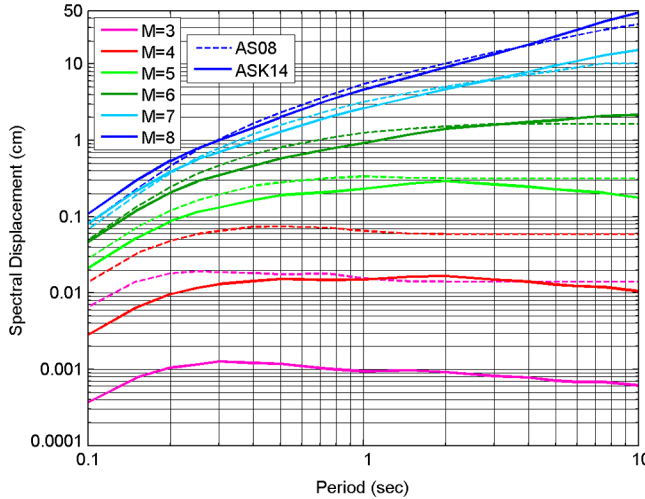


Figure 13. Spectral displacements for a vertical strike slip fault at $R_{JB} = 20$ km and $V_{S30} = 760$ m/s.

nearly constant displacements at long periods, with the corner period (T_D) increasing with increasing magnitude, as expected.

STANDARD DEVIATION

The magnitude dependence of the linear inter- and intra-event standard deviation models (not including the effects of nonlinear site response on the standard deviation) is shown in Figure 14 for $T = 0.2$ s and $T = 1.0$ s. At short periods, the added small-magnitude data has a significantly higher intra-event standard deviation. This

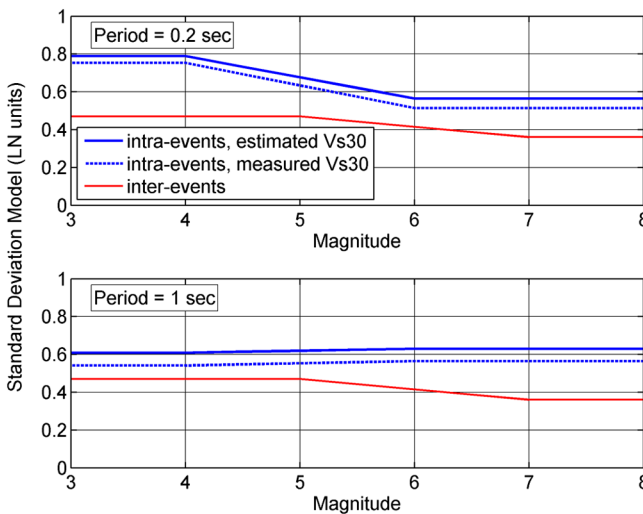


Figure 14. Magnitude scaling of $\phi_{A,L}$ and $\tau_{A,L}$ for $T = 0.2$ s and $T = 1.0$ s.

may be due to an increased effect of the radiation pattern at short periods and short distances from small-magnitude earthquakes. For larger-magnitude earthquakes, which could be considered as many smaller earthquakes combined together, destructive interference of the individual radiation patterns leads to a decreased variability of the ground motions at short distances. The slightly increased inter-event standard deviation for small magnitude could be related to the steeper slope on the magnitude scaling at small magnitudes (see Figure 9), combined with a higher uncertainty when estimating a small-magnitude event (for a detailed description of the effect of measurement errors on the standard deviation, refer to [Abrahamson et al. 2013](#)).

The period dependence of the linear inter-event and intra-event standard deviation models is shown in Figure 15 for magnitudes 5 and 7. Here, the reduction in the intra-event standard deviation for a measured V_{S30} is not constant across the period range, due to the period-dependence of the linear site-response (see Equation 7.6 in [Abrahamson et al. 2013](#)).

The magnitude-dependence of the total standard deviation (combined inter-event and intra-event standard deviations) is shown in Figure 16 for vertical strike-slip earthquakes at a R_{RUP} distance of 30 km and a measured $V_{S30} = 760$ m/s. The standard deviations from the current model are higher than those from [Abrahamson and Silva \(2008\)](#), except for short periods between magnitudes 5 and 6.5. The most significant increase is for the smaller magnitudes, due to the added small-magnitude data, which has very large intra-event variability at short periods.

RANGE OF APPLICABILITY

The model is applicable for distances of 0–300 km and magnitudes 3.0–8.5. Although the largest magnitude in the NGA data set is M 7.9, we consider that the model can be reliably extrapolated to M 8.5. With regards to site conditions, the model is

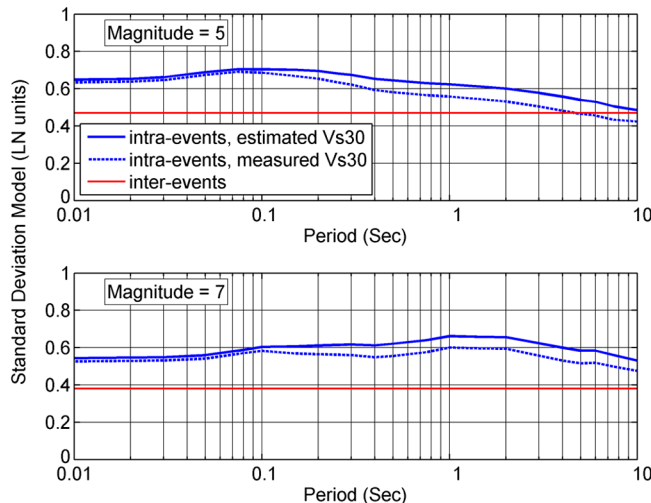


Figure 15. Period dependence of $\phi_{A,L}$ and $\tau_{A,L}$ for magnitudes 5 and 7.

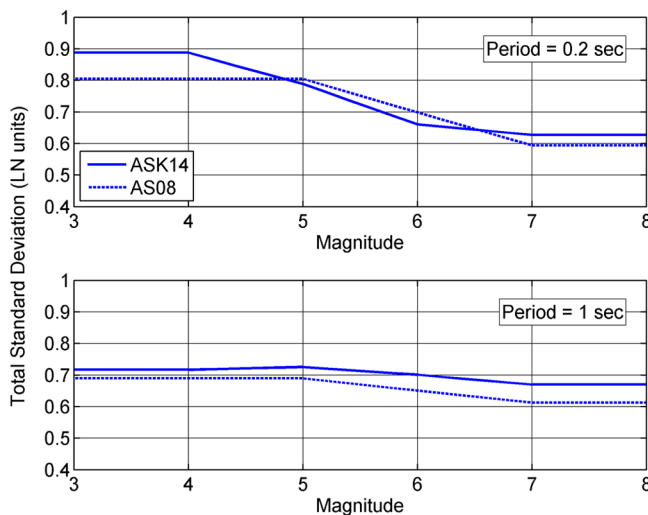


Figure 16. Magnitude dependence of the total standard deviation for a strike-slip event at $R_{RUP} = 30$ km and a measured $V_{S30} = 760$ m/s. Comparison between ASK14 and AS08 for $T = 0.2$ s and $T = 1.0$ s.

considered applicable for $V_{S30} \geq 180$ m/s but it is not well constrained for sites with $V_{S30} \geq 1,000$ m/s. Therefore, for such higher velocities, consider adjusting a better-constrained part of the model (e.g., $V_{S30} = 760$ m/s) using analytical site response methods (such as Kamai et al. 2014).

ACKNOWLEDGMENTS

We would like to acknowledge the other NGA developers and contributors for many fruitful interactions and discussions. We have benefitted from such interactions and adopted some of their concepts and findings in our model.

This study was sponsored by the Pacific Earthquake Engineering Research Center (PEER) and funded by the California Earthquake Authority, California Department of Transportation, and the Pacific Gas & Electric Company. Any opinions, findings, and conclusions or recommendations expressed in this material are those of the authors and do not necessarily reflect those of the above-mentioned agencies.

ELECTRONIC SUPPLEMENTS

Please refer to the online version of this manuscript to access the full set of final model coefficients.

REFERENCES

- Abrahamson, N. A., and Youngs, R. R., 1992. A stable algorithm for regression analyses using the random effects model, *Bull. Seism. Soc. Am.* **82**, 505–510.
- Abrahamson, N. A., and Silva, W. J., 2007. *Abrahamson & Silva NGA Ground Motion Relations for the Geometric Mean Horizontal Component of Peak and Spectral Ground Motion*

- Parameters*, Final report prepared for the Pacific Earthquake Engineering Research Center, October 2007.
- Abrahamson, N. A., and Silva, W. J., 2008. Summary of the Abrahamson & Silva NGA ground motion relations, *Earthquake Spectra* **24**, 67–97.
- Abrahamson, N. A., Silva, W. J., and Kamai, R., 2013. *Update of the AS08 Ground Motion Prediction Equations Based on the NGA-West2 Data Set*, PEER Report No. 2013/04, Pacific Earthquake Engineering Research Center, University of California, Berkeley.
- Al Atik, L., and Abrahamson, N. A., 2010. Nonlinear site response effects on the standard deviations of predicted ground motions, *Bull. Seismol. Soc. Am.* **100**, 1288–1292.
- Ancheta, T. D., Darragh, R. B., Stewart, J. P., Seyhan, E., Silva, W. J., Chiou, B. S.-J., Wooddell, K. E., Graves, R. W., Kottke, A. R., Boore, D. M., Kishida, T., and Donahue, J. L., 2014. NGA-West2 database, *Earthquake Spectra* **30**, 989–1005.
- Boore, D. M., 2010. Orientation-independent, nongeometric-mean measures of seismic intensity from two horizontal components of motion, *Bull. Seismol. Soc. Am.* **100**, 1830–1835.
- Chiou, B. S.-J., and Youngs, R. R., 2014. Update of the Chiou and Youngs NGA model for the average horizontal component of peak ground motion and response spectra, *Earthquake Spectra* **30**, 1117–1153.
- Collins, N., Graves, R., and Somerville, P., 2006. *Revised Analysis of 1-D Rock Simulations for the NGA-E Project*, Final report prepared for the Pacific Earthquake Engineering Research Center, April 2006.
- Donahue, J. L., and Abrahamson, N. A., 2014. Simulation-based hanging wall effects, *Earthquake Spectra* **30**, 1269–1284.
- Gardner, J. K., and Knopoff, L., 1974. Is the sequence of earthquakes in southern California with aftershocks removed, poissonian?, *Bull. Seismol. Soc. Am.* **64**, 1363–1367.
- Kaklamanos, J., Baise, L. G., and Boore, D. M., 2011. Estimating unknown input parameters when implementing the NGA ground motion prediction equations in engineering practice, *Earthquake Spectra* **27**, 1219–1235.
- Kamai, R., Abrahamson, N. A., and Silva, W. J., 2014. Nonlinear horizontal site amplification for constraining the NGA-West2 GMPEs, *Earthquake Spectra* **30**, 1223–1240.
- Wooddell, K. E., and Abrahamson, N. A., 2014. Classification of main shocks and aftershocks in the NGA-West2 database, *Earthquake Spectra* **30**, 1257–1267.

(Received 9 July 2013; accepted 16 January 2014)